# Correlation of structural and few-particle properties of self-organized InAs/GaAs quantum dots

S. Rodt,* A. Schliwa, K. Pötschke, F. Guffarth, and D. Bimberg
*Institut für Festkörperphysik, Technische Universität Berlin, Hardenbergstrasse 36, 10623 Berlin, Germany*
(Received 19 October 2004; published 28 April 2005)

Charged ($X^+$,$X^-$,$XX^+$) and neutral ($X$,$XX$) exciton complexes in single InAs/GaAs quantum dots (QDs) are investigated by cathodoluminescence spectroscopy. The relative spectral positions of the few-particle transition energies compared to the $X$ transition are shown to be strongly correlated to the QD size. Starting from an unprecedented detailed knowledge about the size, shape, and composition of the investigated quantum dots these energies are calculated using an eight-band $\mathbf{k}\cdot\mathbf{p}$ theory for the single-particle states and the configuration interaction method for the few-particle states. The observed strong variation of the few-particle energy positions is found to originate from a depletion of the number of excited states in the QDs when they become smaller. Then the degree of correlation is reduced. From a detailed comparison of the numerical results with the experimental data we identify the number of hole states bound in the QD to be the key parameter for size and sign variations of the relative few-particle energies.

DOI: 10.1103/PhysRevB.71.155325 PACS number(s): 78.67.Hc, 73.21.La, 71.45.Gm, 78.60.Hk

## I. INTRODUCTION

Comparing the details of the calculated and measured few-particle spectra of single quantum dots (QDs) is difficult due to the uncertainty about the actual structure and chemical composition of the probed QD.[1] Still, the most advanced techniques able to yield information on an atomic scale on single QDs do not suffice. They either provide a snapshot of the shape of an uncapped QD after cooling the whole layer [scanning tunneling microscopy (STM) (Ref. 2) or atomic force microscopy (AFM)] or just a cross section of the shape of the QD and the arrangement of the various atoms at an unknown position [cross section STM ($X$STM) (Ref. 3)]. Even if the complete three-dimensional distribution of atoms in a QD could be assessed, it could not be correlated in detail to its spectroscopic signature due to dot-to-dot shape, size, and composition variations. This problem can be solved based on a radically different approach by exploiting the multimodal dot-size distributions recently identified via photoluminescence (PL) spectroscopy of appropriately grown samples.[4,5] The samples were grown by metal-organic chemical-vapor deposition (MOCVD) using Sb as a surfactant.

Low-excitation PL leads to the identification of up to eight subensembles, each showing a much-reduced spectral width ($\sim$30 meV) as compared to the original ensemble. The detailed analysis of the PL spectra and transmission electron microscopy (TEM) data demonstrates that (i) the QDs are relatively flat, (ii) the QDs have a well-defined upper (001) interface, and (iii) each peak represents a subensemble of QDs sharing the same size and shape. With decreasing photon energy the size of each QD subensemble increases by exactly one monolayer. Thus the QDs show a shell-like formation with an increasing height- to base-length aspect ratio with increasing QD size.[5]

Realistic calculations based on an eight-band $\mathbf{k}\cdot\mathbf{p}$ model demonstrate very good agreement with the experimental results, assuming truncated pyramidal InAs/GaAs QDs and allow the detailed indentification of the evolution of QD height and base length in monolayer steps from one subensemble to the next.[5]

Given this knowledge, the fundamental features of single and multiple excitons derived from single-dot spectra can be correlated to and derived from our detailed knowledge of the QD structure. These spectra, revealing the essentials of few-particle effects, are obtained from cathodoluminescence measurements using near-field shadow masks.[6] In Ref. 7 we have reported and analyzed as a first result of our investigations a transition from positive to negative biexciton binding energies with increasing exciton recombination energy. Here we focus on the negatively and positively charged excitons (trions) and the positively charged biexciton.

It should be pointed out that due to the fast deposition rate and the use of antimony as a surfactant the structural and therefore optical properties of our MOCVD-grown samples are fairly different from typical In(Ga)As/GaAs-QDs as grown by molecular-beam-epitaxy (MBE). Hence it is no surprise that the spectroscopic shifts observed in single-dot spectroscopy on MBE-grown QDs[8–14] are different from the values reported in this paper.

Some typical data for negatively and positively charged trions are compiled in Table I and compared to our data. The origin of the trion's spectroscopic shifts is traced to an imbalance of the direct Coulomb terms $J_{e_0e_0}$, $J_{e_0h_0}$, and $J_{h_0h_0}$[15] being related to a difference in the extension of the ground-state electron and hole wave functions. Hence, the much larger trion shifts in our case point to a larger difference in electron and hole localizations in the MOCVD-grown QDs.

Calculations using the configuration-interaction method can account for exchange and correlation effects and are applied to yield detailed insight into the close interrelation between structural and few-particle properties. An understanding is achieved in terms of the subsequent delocalization of excited hole states with decreasing dot size. It is demonstrated that the number of bound *electron* states cannot account for the observed few-particle energies, whereas the number of bound hole states does.

 

TABLE I. Available experimental results on the energy difference between the exciton and the two different trions $X^-$ and $X^+$, arranged according to the growth method.

| | QD-material | Growth-method | $X^0-X^-$ [meV] | $X^0-X^+$ [meV] |
|---|---|---|---|---|
| Refs. 8–14 | In(Ga)As | MBE | 3.1–6.1 | −1−−3.3 |
| This paper | InAs | MOCVD | 7.8–9.0 | −2.0−−14.0 |

## II. SAMPLE GROWTH

The investigated samples were grown by metal-organic chemical-vapor deposition (MOCVD) on GaAs(001) substrates. Trimethylindium, trimethylgallium, tertiarybutylarsine, and triethylantimony were used as precursors. At 625 °C a 300-nm-thick GaAs buffer layer followed by a 60-nm $Al_{0.6}Ga_{0.4}As$ diffusion barrier and 90-nm GaAs were grown. For the growth of the QD layer the growth temperature was reduced to 485 °C before depositing about 1.9-monolayer (ML) InAs followed by a 5-s growth interruption. Subsequently, the QDs were capped with 50 nm of GaAs; the first 5 nm were grown at 485 °C and then the temperature was ramped to 600 °C. Finally, a 20-nm $Al_{0.33}Ga_{0.67}As$ diffusion barrier and a 10-nm GaAs capping layer were deposited. Antimony was added during the deposition of the InAs layer and the growth interruption. Antimony is not incorporated into the QDs due to its large size, but it acts as a surfactant, modifying the evolution of the InAs QDs.[16]

## III. DETERMINATION OF QD MORPHOLOGY AND THE SPECTRUM OF EXCITED STATES

TEM investigations of our samples reveal a flat, truncated shape of the QDs with a density of about $\sim 4\times 10^{10}$ cm$^{-2}$. A more detailed insight into the QD structure is obtained by exploiting the multimodal splitting of the photoluminescence spectra.[4] The QD ensemble consists of up to eight subensembles showing narrow spectral width of ~30 meV each. This splitting is attributed to a monolayer change of the QD size from subensemble to subensemble,[5] allowing us to determine, e.g., the QD height of a given subensemble just by counting the number of adjacent peaks. From the optical measurements it can also be concluded that the QDs consist of practically ideal InAs.[5]

The spectrum of excited states is investigated by photoluminescence excitation (PLE) spectroscopy. QDs having a height $\geqslant$7 MLs do show first and second excited state transitions in absorption. QDs having a 4–6-ML height show only one excited state transition. Smaller QDs show no excited states at all.[4] As will be discussed later, this observation will be of the largest importance for quantifying the impact of correlation energy on the spectral position of the few-particle states.

## IV. SINGLE-DOT SPECTRA OBTAINED FROM CATHODOLUMINESCENCE SPECTROSCOPY

Single QDs were probed in a cathodoluminescence (CL) setup. The samples were mounted on the cold finger of a He-flow cryostat in a JEOL JSM 840 scanning electron microscope. The acceleration voltage was 7 kV. The luminescence was dispersed by a 0.3-m spectrometer equipped with a 1200 grooves/mm grating and detected by a liquid-nitrogen-cooled (LN-cooled) Si-CCD. At 1.28 eV the minimal full width at half maximum (FWHM) as given by the setup was ~140 $\mu$eV. Due to the spectral sensitivity of the detector only luminescence with energies $\geqslant$1.2 eV can be investigated. To reduce the number of simultaneously probed QDs a Au shadow mask was evaporated onto the sample surface, having apertures of ~100 nm in diameter. For that size and a QD density of $4\times 10^{10}$ cm$^{-2}$ about four QDs are probed on average.

A representative CL spectrum, as shown in Fig. 1(a), consists of a rather large number of sharp lines that might originate from various few-particle complexes in different QDs. Therefore, first of all, the lines stemming from the same QD must be identified. After having done this, the lines from one QD need to be attributed to the recombination of various few-particle states such as exciton ($X$), positive or negative trion ($X^+$ or $X^-$), biexciton ($XX$), or charged biexciton ($XX^{+/-}$).

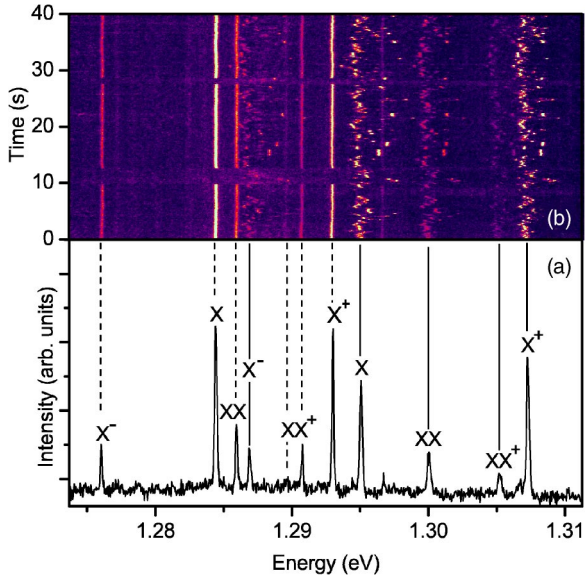


FIG. 1. (Color online) (a) A typical spectrum as measured through a 100-nm aperture. (b) Temporal evolution of (a) consisting of 500 spectra, each being integrated for 80 ms. The spectral jitter allows us to identify two overlapping single-QD spectra marked by dashed ($QD_1$) and full ($QD_2$) lines in (a). The different recombinations are marked as follows. $X$: exciton; $XX$: biexciton; $X^{+/-}$: positively/negatively charged exciton (trion); $XX^+$: positively charged biexciton.

The first step of identification, the discrimination of spectra from different dots, is based on the omnipresent spectral jitter[17] of the transition energies. The statistical variations of the local electric field cause energy variations via the quantum-confined Stark effect, leading to a spectral jitter that is different for each QD [Fig. 1(b)].

Next the spectral lines from one QD need to be identified. The *exciton* and *biexciton* emissions are cross-polarized doublets of identical splitting but reversed polarization with respect to [110] as outlined in Ref. 7. The observed splittings between 60 and 134 $\mu$eV are attributed to the fine-structure splitting of the bright exciton state caused by the $C_{2v}$ symmetry of the confinement potential, resulting from the piezoelectric potential[18] and (or) a possible lateral QD elongation.[19] The exciton and biexciton emissions are distinguished by their characteristic excitation-density dependences. The effective excitation density was varied by scanning the electron beam across the aperture and using the integrated intensity as a reference. The exciton first appears with a slope of $\sim$1, whereas the biexciton intensity depends quadratically on the excitation density.[20]

The complete lack of a measurable fine structure of the other emissions indicates the recombination of *trions* and higher-charged exciton complexes, for which either the electron or hole spin is paired off, thus quenching the exchange interaction. Charged exciton complexes have been investigated in detail recently.[8–14] The identification of the trions as being positive or negative is not obvious or trivial. Their intensity is, however, a function of the background doping: Increased *p*-type doping, for instance, results in a stronger emission from positive trions, as is confirmed here by extra samples.

At higher excitation densities even the recombination of a *positively charged biexciton doublet* ($XX^+$) is observed. The two lines of $XX^+$ exhibit a fixed-intensity ratio as a function of the excitation intensity, pointing at a same origin of both lines. Since this particle has more than one recombination channel, polarization is expected[21] and observed by us (not shown here).

Figure 2 shows two single-QD spectra. The upper spectrum shows an intense luminescence from positively charged complexes, and the lower spectrum stems from a QD for which also $X^-$ can be observed. The probability of probing a negatively charged, neutral, or positively charged QD depends on the background doping, as mentioned before. The larger diffusion length of electrons can be utilized additionally to identify $X^-$ by placing the electron beam at an appropriate distance to the QD.

This identification procedure has been performed for more than 70 single-dot spectra and the resulting energy differences between the few-particle states are plotted in Fig. 3 with respect to the single-exciton recombination energy.

## V. RESULTS AND INTERPRETATION

Figure 3 shows (a) the negative trion is always redshifted compared to the exciton, whereas the positive one is blueshifted; (b) the biexciton turns from binding (i.e., redshifted) to antibinding with increasing exciton energy;[7] (c) the negative trion and the exciton have similar slopes (containing each only one hole). The positive trion and biexciton slopes are parallel with both having two occupied hole states; and (d) there is no charged biexciton found above 1.325 eV.

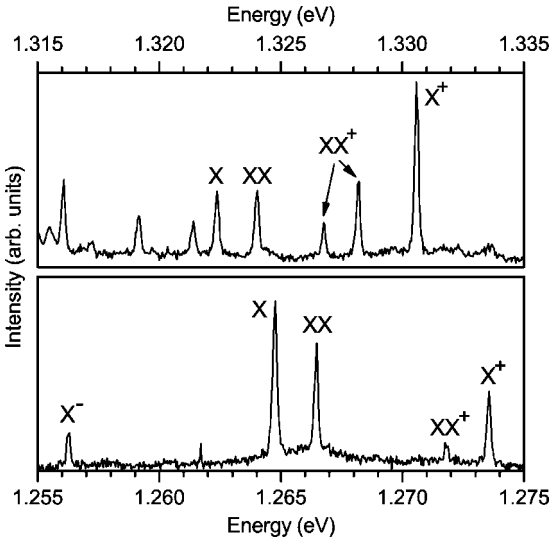


FIG. 2. Two single-QD spectra as identified by the spectral jitter. *X*: exciton; *XX*: biexciton; $X^{+/-}$: charged excitons; $XX^+$: charged biexciton. The unmarked lines do belong to different QDs. The upper spectrum demonstrates a predominantly positively charged QD with no $X^-$ emission, whereas the lower spectrum shows a QD with emission from $X^-$ also.

To understand these findings configuration interaction (CI) calculations were carried out. The underlying single-particle states were obtained by eight-band $\mathbf{k}\cdot\mathbf{p}$ theory (see Appendix). As model structures, pure InAs QDs of (truncated) pyramidal shape in GaAs were chosen [see Sec. III and Figs. 4(d11), 4(d12), 4(d21), and 4(d22)]. The relative positions of the few-particle transition lines are primarily determined by the direct Coulomb interaction and the degree of correlation.[22] The former depends on the relative size and shape of the wave functions and their mutual positions in the QD, while the latter is ruled by the number of bound electron

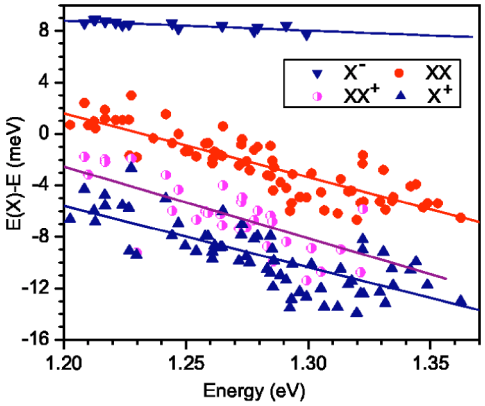


FIG. 3. (Color online) Energy distances between the recombination energy of the few-particle states as a function of and relative to the neutral-exciton recombination energy. The straight lines are linear fits as guides for the eyes.

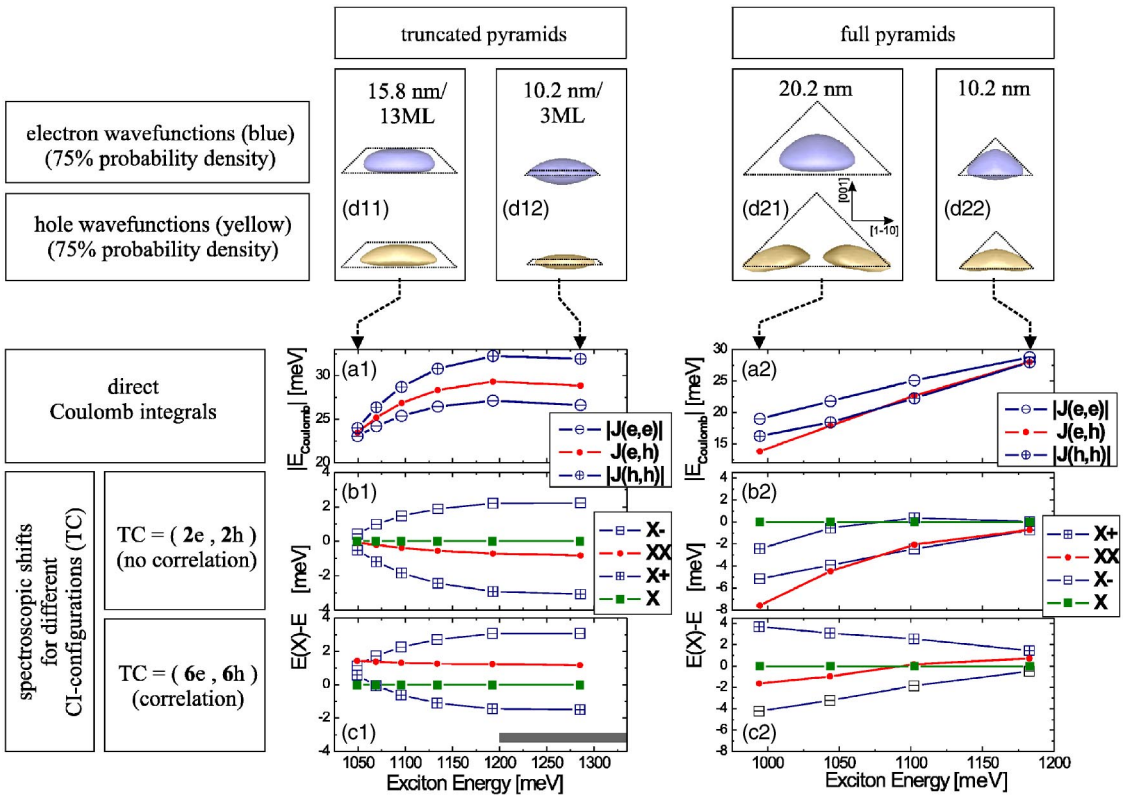


FIG. 4. (Color online) (a) Absolute Coulomb charging and exciton binding energies for the truncated pyramidal (*a*1) and the pyramidal-shaped (*a*2) QDs. (b) and (c) The predicted few-particle energies (relative to the exciton transition energy) for these structures. While in graph (b) the correlation effects are removed in that a ground state configuration (2,2) is applied, in graph (c) the configuration (6,6) corresponds to six bound electron and hole states (i.e., three electron and hole levels), thus accounting for a fixed degree of correlation.

and hole states in the QD potential and is influenced by the energy-level spacing. For a deeper understanding these effects are investigated separately in the following way: direct Coulomb effects including exchange are calculated by using only the ground-state configuration in the CI basis for diagonalizing the various few-particle Hamiltonians. This procedure is close to first-order perturbation theory. To mimic second-order perturbation theory,[22] and include correlation effects, those configurations are also considered that originate from excited states. At the end the full configuration-interaction model is applied.

### A. Direct Coulomb interaction

In Fig. 4(a1) the absolute, direct Coulomb energies are plotted against the exciton energy for the truncated pyramidal QDs discussed in Sec. III. For the smallest QD, having an exciton energy of 1280 meV, we find a large difference between the Coulomb charging energy of electrons and holes of ~6 meV. The exciton binding energy ranges between these two values. This result is different from the situation in large pyramidal QDs (base length ~20.2 nm) [Fig. 4(a2)], where the Coulomb charging energy of the electron (*e*) ground states is larger than for the hole (*h*) ground states, and the exciton binding energy is even smaller. All these effects can be traced back to the wave-function shape; the Coulomb charging energy depends on how strongly a particle is localized, and the exciton binding energy is a function of the spatial electron-hole (*e*-*h*) overlap. While in the case of a very small QD [Fig. 4(d12)] the hole ground state is much more strongly localized than the electron ground state, in the large pyramid [Fig. 4(d21)] the hole wave function is strongly elongated along the [110] direction due to a large piezoelectric field with a density minimum in the center of the dot.[18] The electron ground state is less sensitive to the piezoelectric potential due to the smaller electron mass. Thus in the first case of a tiny, flat QD the hole ground state is spatially more concentrated, than the electron counterpart, with an optimal wave-function overlap. In the other case of a large, full pyramid, however, the electron is more strongly localized than the hole, thereby having a poor electron-hole overlap, resulting in a smaller exciton binding energy.

The resulting emission energies of biexcitons and trions relative to the exciton, as plotted in Fig. 4(b1), reflect the Coulomb interaction within the few-particle complexes and exchange effects. To switch off the correlation effects (which are separately considered in the next section), only the ground states are considered to build up the CI basis (see Appendix). The positive trion is blueshifted compared to the exciton, since the additional *h*-*h* Coulomb charging outweighs the extra *e*-*h* attraction. The opposite holds for the negative trion for similar reasons. The biexciton can never be redshifted (i.e., binding) compared to the exciton if correlation effects are omitted.

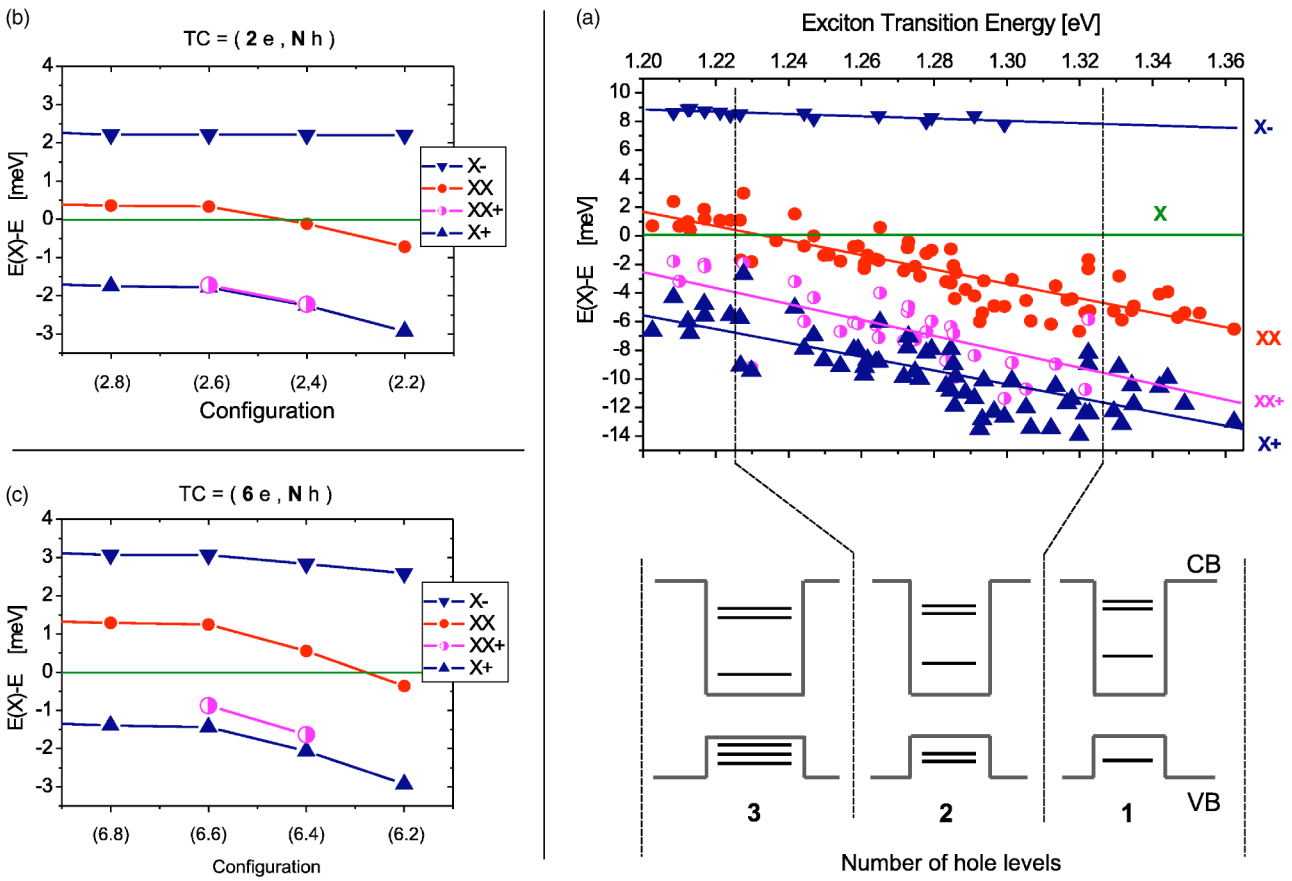


FIG. 5. (Color online) Comparison between measured (a) and calculated (b) and (c) spectroscopic shifts. The calculation is done for different CI configurations. The number of electron states the CI accounts for is fixed at two in panel (b) and at six in (c), whereas the number of hole states is being varied in the range between eight and two.

The same mechanism applies to the pyramidal QDs in Fig. 4(b2). For the large one we find blueshifted biexciton and trion lines, since the repulsive Coulomb charging energies predominate over the attractive electron-hole binding energies. The trion lines change their energetic positions [compared to Fig. 4(b1)] since the *e-e* repulsion is greater than that of *h-h*.

To summarize this section the finding (a) (see first paragraph of Sec. V) regarding the relative energetic positions of excitons and trions can be understood in terms of direct Coulomb interactions alone. The remaining points (b) and (c) will be discussed next in terms of correlation effects.

### B. Correlation

As discussed before, the number of bound states is not the same for all QDs, but decreases with decreasing QD size. Now correlation is incorporated (and can be varied) via the number of included electron and hole states to build up the basis of the Slater determinants that the CI method rests on. The result is plotted in Fig. 4(c1) for a total configuration (see Appendix) of $TC=(6,6)$. Compared to Fig. 4(b1) the biexciton turns from antibinding to binding (i.e., from blueshifted to redshifted compared to the exciton line) for *all* truncated pyramid structures. In the experiment, however, we find a transition from a binding to an antibinding biexciton within a very small energy range marked by the gray bar in Fig. 4(c1). Thus we follow our conclusion from Ref. 7 and attribute this transition to the successive delocalization of bound states. Here we extend this investigation to find out whether the electron or the hole states or both are affected. In the CI scheme this can be emulated by choosing different configurations. In a $TC=(2,6)$, for example, two electron and six hole states are assumed as being bound in the QD. Figures 5(b) and 5(c) show the results obtained for one QD (11.3 nm base length and 5 ML height) using different configurations. While the number of bound electron states is fixed to two in 5(b) and six in 5(c), the number of hole states is varied in each plot. If the $TC=(6,6)$ in graph 5(c) is assigned to the QDs found at the energy of 1.2 eV in 5(a) and $TC=(6,2)$ to those in the energy range around 1.35 eV a good agreement is found. This implies that in the investigated energy region the number of bound electron states does not account for the observed trend and that the number of hole states decreases from six down to two (as depicted by the sketch in Fig. 5). This finding is strongly supported by the disappearance of the positively charged biexciton ($XX^+$) (Fig. 3, half-filled circles) line at around 1.32 eV, since that line is tied to the existence of at least three bound hole levels.

TABLE II. Relation between particle type, basis size, number of matrix elements (ME) and number of *nonzero* ME if six electron and ten hole states contribute to the total configuration.

| Particle type | Basis size | No. of ME | No. of *nonzero* ME |
|---|---|---|---|
| $X$ | 60 | 3600 | 1830 |
| $X^-$ | 150 | 22 500 | 7275 |
| $X^+$ | 270 | 72 900 | 17 685 |
| $XX$ | 675 | 455 625 | 63 450 |

## VI. CONCLUSION

We have investigated recombinations from charged and neutral exciton complexes in self-organized InAs/GaAs QDs as a function of the single-exciton recombination energy. The relative recombination energies of all investigated complexes ($X^-$,$X^+$,$XX$,$XX^+$) were found to decrease for an increasing exciton recombination energy, but with different slopes. Correlation was identified as the origin of the decrease: QDs with larger exciton-recombination energy show a smaller number of bound states reducing the effects of correlation, thus shifting the relative recombination energy to smaller values. By separately varying the number of bound electron and hole states we found out that only by decreasing the number of hole states can the experimentally found slopes be theoretically reproduced. We conclude that the number of bound-hole states is reduced here from six to two in the investigated energy range. This conclusion is also supported by our PLE results and the disappearance of $XX^+$ for the high-energy QDs for which at least three bound-hole levels are needed. The number of bound electron states was found to play only a minor role for correlation.

## ACKNOWLEDGMENTS

We thank N. Zakharov and P. Werner for TEM measurements. The electronic-structure calculations were performed on the IBM pSeries 690 supercomputer at HLRN within Project No. bep00014. Parts of this work were supported by Deutsche Forschungsgemeinschaft in the framework of SFB 296, by INTAS project No. 99-00928, and by the SANDiE Network of Excellence of the European Commission, Contract No. NMP4-CT-2004-500101.

## APPENDIX: FEW-PARTICLE STATES: FULL CONFIGURATION-INTERACTION METHOD

This appendix outlines how few-particle energies are calculated using the configuration-interaction (CI) method. First, the single-particle states $\phi_e^i$ and $\phi_h^j$ (resulting from the eight-band $\mathbf{k}\cdot\mathbf{p}$ model) are used as building blocks for creating the CI basis. For an exciton this results in

$$[\phi_e^i(\mathbf{r}),\phi_h^j(\mathbf{r})] \mapsto \mathcal{A}[\phi_e^i(\mathbf{r})\phi_h^j(\mathbf{r}')] = \frac{1}{\sqrt{2}}[\phi_e^i(\mathbf{r})\phi_h^j(\mathbf{r}') - \phi_h^j(\mathbf{r})\phi_e^i(\mathbf{r}')], \quad \text{(A1)}$$

where $\mathcal{A}$ is the antisymmetrization operator and $i$ ($j$) is running over the number of bound electron (hole) states. The pair $(i,j)$ will be called the (total) configuration (TC) and is responsible for the degree of correlation the CI scheme can cover. The exciton eigenenergies are obtained by diagonalizing the two-particle Hamiltonian,

$$H(\mathbf{r},\mathbf{r}') = H(\mathbf{r}) + H(\mathbf{r}') + C(\mathbf{r},\mathbf{r}') \quad \text{(A2)}$$

within the CI basis. $H(\mathbf{r})$ and $H(\mathbf{r}')$ are the single-particle Hamiltonians acting on the first and the second subspaces, respectively. $C(\mathbf{r},\mathbf{r}')$ is the two-particle Coulomb operator acting on both subspaces, and thus being responsible for the renormalization. For TC=(2,2) only the ground states are considered, and thus no correlation but only exchange (since the basis is antisymmetric) is present. In TC=(6,2) two excited electron levels (each level being twofold spin degenerate) are added. Each electron-hole level pair establishes a subconfiguration (SC), and the Coulomb mediated interaction between these (here three) subconfigurations is responsible for the correlation and the origin of the notion of *configuration interaction*.

A similar procedure is applied for the trion and biexciton states. To summarize this part, a CI calculation starts with a decision on the number of occupied states, determining the few-particle type, and on the number of bound states to include in building up the basis. Provided the basis states are antisymmetric, CI accounts for the exchange effects, and if the basis is sufficiently large, the correlation effects are included. In contrast to the Hartree-Fock method, CI offers access to the excited states. The disadvantage is the factorial growth of the number of Slater determinants with the number of occupied states. Table II gives an impression if six electron- and ten hole states contribute to the TC.

*Electronic address: srodt@physik.TU-Berlin.DE

[1] D. Bimberg, M. Grundmann, and N. N. Ledentsov, *Quantum Dot Heterostructures* (Wiley, Chichester, 1999).
[2] J. Márquez, L. Geelhaar, and K. Jacobi, Appl. Phys. Lett. **78**, 2309 (2001).
[3] H. Eisele, O. Flebbe, T. Kalka, C. Preinesberger, F. Heinrichsdorff, A. Krost, D. Bimberg, and M. Dähne-Prietsch, Appl. Phys. Lett. **75**, 106 (1999).
[4] F. Guffarth, R. Heitz, A. Schliwa, K. Pötschke, and D. Bimberg, Physica E (Amsterdam) **21**, 326 (2004).
[5] R. Heitz, F. Guffarth, K. Pötschke, A. Schliwa, D. Bimberg, N. D. Zakharov, and P. Werner, Phys. Rev. B **71**, 045325 (2005).
[6] S. Rodt, A. Schliwa, R. Heitz, V. Türck, O. Stier, R. L. Sellin, M. Strassburg, U. W. Pohl, and D. Bimberg, Phys. Status Solidi B **234**, 354 (2002).
[7] S. Rodt, R. Heitz, A. Schliwa, R. L. Sellin, F. Guffarth, and D. Bimberg, Phys. Rev. B **68**, 035331 (2003).
[8] D. V. Regelman, E. Dekel, D. Gershoni, E. Ehrenfreund, A. J. Williamson, J. Shumway, A. Zunger, W. V. Schoenfeld, and P. M. Petroff, Phys. Rev. B **64**, 165301 (2001).
[9] J. J. Finley, P. W. Fry, A. D. Ashmore, A. Lemaître, A. I. Tartakovskii, R. Oulton, D. J. Mowbray, M. S. Skolnick, M. Hopkinson, P. D. Buckle, and P. A. Maksym, Phys. Rev. B **63**, 161305 (2001).
[10] F. Findeis, M. Baier, E. Beham, A. Zrenner, and G. Abstreiter, Appl. Phys. Lett. **78**, 2958 (2001).
[11] F. Findeis, M. Baier, A. Zrenner, M. Bichler, G. Abstreiter, U. Hohenester, and E. Molinari, Phys. Rev. B **63**, 121309 (2001).
[12] M. Baier, F. Findeis, A. Zrenner, M. Bichler, and G. Abstreiter, Phys. Rev. B **64**, 195326 (2001).
[13] R. Heitz, T. Warming, F. Guffarth, C. Kapteyn, P. Brunkov, V. M. Ustinov and D. Bimberg, Physica E (Amsterdam) **21**, 215 (2004).
[14] E. S. Moskalenko, V. Donchev, K. F. Karlsson, P. O. Holtz, B. Monemar, W. V. Schoenfeld, J. M. Garcia, and P. M. Petroff, Phys. Rev. B **68**, 155317 (2003).
[15] G. Bester and A. Zunger, Phys. Rev. B **68**, 073309 (2003).
[16] X. Yang, M. J. Jurkovic, J. B. Heroux, and W. I. Wang, Appl. Phys. Lett. **75**, 178 (1999).
[17] V. Türck, S. Rodt, O. Stier, R. Heitz, R. Engelhardt, U. W. Pohl, D. Bimberg, and R. Steingrüber, Phys. Rev. B **61**, 9944 (2000).
[18] O. Stier, M. Grundmann, and D. Bimberg, Phys. Rev. B **59**, 5688 (1999).
[19] V. D. Kulakovskii, G. Bacher, R. Weigand, T. Kümmell, A. Forchel, E. Borovitskaya, K. Leonardi, and D. Hommel, Phys. Rev. Lett. **82**, 1780 (1999).
[20] M. Grundmann and D. Bimberg, Phys. Rev. B **55**, 9740 (1997).
[21] I. A. Akimov, A. Hundt, T. Flissikowski, and F. Henneberger, Appl. Phys. Lett. **81**, 4730 (2002).
[22] P. Lelong and G. Bastard, Solid State Commun. **9**, 819 (1996).